Journal of Volcanology and Geothermal Research 295 (2015) 43–54

Contents lists available at ScienceDirect

Journal of Volcanology and Geothermal Research

journal homepage: www.elsevier.com/locate/jvolgeores

Terrestrial laser scanning observations of geomorphic changes and varying lava lake levels at Erebus volcano, Antarctica

Laura K. Jones [a], Philip R. Kyle [a,*], Clive Oppenheimer [b], Jedediah D. Frechette [c], Marianne H. Okal [d]

[a] Department of Earth and Environmental Science, New Mexico Institute of Mining and Technology, Socorro, NM 87801, USA
[b] Department of Geography, University of Cambridge, Downing Place, Cambridge CB2 3EN, UK
[c] Department of Earth and Planetary Science, University of New Mexico, Albuquerque, NM 87131, USA
[d] UNAVCO, 6350 Nautilus Drive, Boulder, CO 80301-5394, USA

ARTICLE INFO

Article history:
Received 13 October 2014
Accepted 25 February 2015
Available online 6 March 2015

Keywords:
Erebus
TLS
Lidar
Geomorphology
Lava lake

ABSTRACT

A Terrestrial Laser Scanning (TLS) instrument was used to image the topography of the Main Crater at Erebus volcano each December in 2008, 2009, and 2010. Our high-spatial resolution TLS scans provide unique insights into annual and decadal scale geomorphic evolution of the summit area when integrated with comparable data collected by an airborne instrument in 2001. We observe both a pattern of subsidence within the Inner Crater of the volcano and an ~3 m per-year drop in the lava lake level over the same time period that are suggestive of decreasing overpressure in an underlying magma reservoir. We also scanned the active phonolite lava lake hosted within the Inner Crater, and recorded rapid cyclic fluctuations in the level of the lake. These were sporadically interrupted by minor explosions by bursting gas bubbles at the lake surface. The TLS data permit calculation of lake level rise and fall speeds and associated rates of volumetric change within the lake. These new observations, when considered with prior determinations of rates of lake surface motion and gas output, are indicative of unsteady magma flow in the conduit and its associated variability in gas volume fraction.

1. Introduction

Terrestrial Laser Scanning (TLS), based on time-of-flight light detection and ranging (lidar) technology, is finding widespread application in the geosciences including volcanology (e.g., Tarolli, 2014). Current TLS systems are capable of imaging meter to kilometer-scale areas with centimeter to sub-centimeter precision. TLS mapping and repeat surveys have been applied to geomorphic studies of volcanoes and volcanic terrains (Pesci et al., 2007; Tarquini et al., 2012; Pesci et al., 2013), mapping and characterization of both ancient and active lava flows (James et al., 2009; Nelson et al., 2011; Cashman et al., 2013); in geotechnical studies of slope stability (Nguyen et al., 2011; Norini and Acocella, 2011); and glaciological impacts of tephra fallout (Nield et al., 2013).

Here, we use TLS to study the timescales of both rapid (seconds) and prolonged (years) changes at Erebus volcano, Antarctica each December in 2008, 2009 and 2010. To extend the time interval of the study, we integrate the TLS data with Airborne Laser Scanner (ALS) observations acquired in 2001 (Csatho et al., 2008). Our primary objective was to determine if short-term changes in lava lake level might correlate with ~10 min cycles seen in surface motion of the lake (Oppenheimer et al., 2009; Peters et al., 2014b) and in gas chemistry and fluxes (Boichu et al., 2010; Peters et al., 2014a). A secondary objective was to map the topography of the Inner Crater in order to identify geomorphic changes, such as ground deformation and talus accumulation, which occur between field seasons. While Erebus has been visited annually since the 1970s, few coherent observations have been made to assess the style and rates of geomorphic change within the crater. This study presents a detailed assessment of the processes shaping the dynamic topography of the Erebus crater, and reports on the applications of TLS to monitor the activity of an active lava lake.

2. Erebus summit area and lava lake

Erebus is a large (~2000 km^3) alkaline stratovolcano located on Ross Island, Antarctica (77°32′ S, 167°10′ E), with a summit elevation of 3794 m (Esser et al., 2004). The summit region of Erebus volcano above 3200 m, is a plateau nearly 4 km in diameter, representing the remnants of two episodes of caldera collapse dated between 80–24 ka and 25–11 ka ago (Harpel et al., 2004; Kelly et al., 2008), and subsequent infilling with younger lava flows. Currently, this summit plateau also contains two craters: the Main Crater (600 m × 470 m), which hosts the phonolite lava lake, and the Side Crater (250 m across), which contains areas of hot ground (Csatho et al., 2008; Fig. 1). The lava lake resides in the Inner Crater, which is a pit within the Main

* Corresponding author. Tel.: +1 505 385 1117; fax: +1 575 835 5634.
E-mail addresses: lkzjones@gmail.com (L.K. Jones), kyle@nmt.edu (P.R. Kyle), co200@cam.ac.uk (C. Oppenheimer), jedfrechette@gmail.com (J.D. Frechette).

http://dx.doi.org/10.1016/j.jvolgeores.2015.02.011
0377-0273/

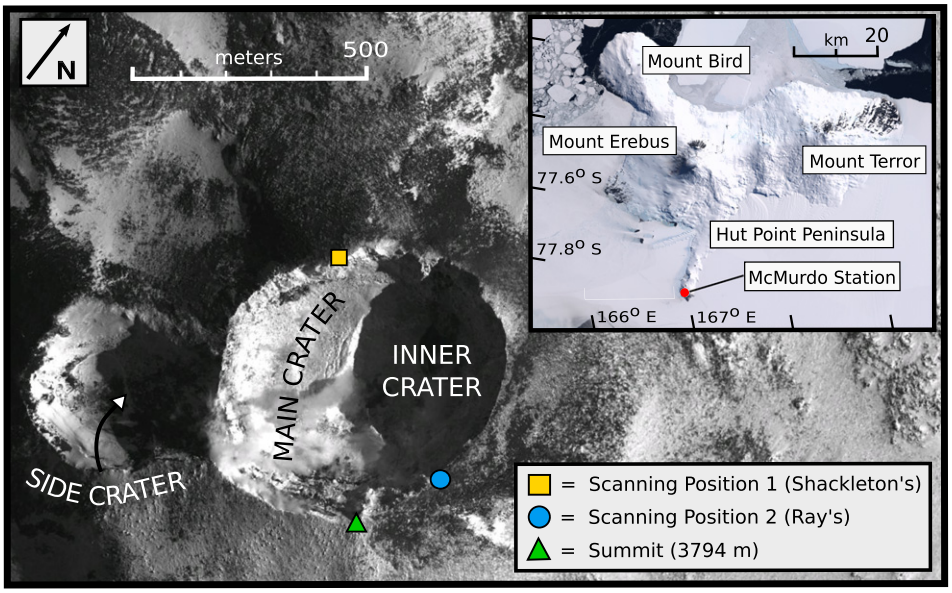

Fig. 1. View of the Erebus summit area showing the locations of the Main, Inner and Side Craters and the positions from which the terrestrial laser scans were acquired. Inset shows Ross Island, Mount Erebus, and other key features of the island not discussed in the text.

Crater (Fig. 1). The Main Crater also contains fumaroles and areas of steaming ground. In contrast to other lava lakes around the world, the Erebus lava lake is composed of evolved anorthoclase-bearing phonolite magma produced by 75% fractional crystallization of a mantle-derived parental basanite magma (Kyle et al., 1992). As a consequence of its phonolitic composition the magma is more viscous than typical basalts (Le Losq et al., 2015), and has a distinctive rheology. Most notably, the Erebus lava lake is the site of sporadic explosions associated with the rupture of large gas bubbles (Dibble et al., 2008). The gas composition in the bubbles is significantly more CO_2-rich than the passively emitted gases from the lake (Oppenheimer et al., 2011; Burgisser et al., 2012).

A number of works have reported on quasi-periodic behavior of the Erebus lava lake. Cycles and variations in SO_2 emission rates were reported by Kyle et al. (1994) and further quantified by Sweeney et al. (2008). Oppenheimer et al. (2009) made observations of corresponding lake surface velocity and gas geochemical cycles. Peters et al. (2014a,b) demonstrated the persistence of the cycles and correlations of lake surface speed, lake level, gas flux, radiative output, and gas composition. More detailed analyses of the variations in gas compositions measured by Fourier transform infrared spectroscopy during the cycles are described by Ilanko et al. (2015).

Several pertinent observations can be drawn from these observations of gas and thermal studies: (1) the cyclic behavior is a prevalent and persistent mode of the lava lake, and is only ephemerally perturbed (for a few minutes) by the rupture of bubbles (even large decametric ones) at the lake surface; (2) the period of cycles varies by over a factor of two but is approximately 10 min; (3) change in lake level slightly precedes (by 1–3 min; Peters et al., 2014b) change in the mean speed of the lake surface (in the horizontal plane) and in gas ratios; (4) the quantity of gas released during a cycle (Boichu et al., 2010; Peters et al, 2014a) represents a volume an order of magnitude greater than the volumetric change associated with half a cycle (the net volume change during a whole cycle is zero); (5) the variations in gas composition appear to reflect subtle variations in redox conditions (Aletti et al., 2014; Peters et al., 2014a; Ilanko et al., 2015) that may be associated with degassing of sulfur from the magma (Moussallam et al., 2014); and (6) the timing of the arrival of gas bubbles with diameters of a few m at the surface appears independent of the phase of the cycles (Peters et al., 2014b). It is with this background that we examine high precise TLS observations of lava lake levels.

3. TLS data collection and processing

3.1. Instrumentation and data collection

We acquired TLS surveys of the Main Crater on Erebus volcano using an Optech ILRIS-3D ER (Extended Range) lidar. This instrument uses a 1535 nm wavelength (near infrared) laser and has a sampling frequency of 2.5–3.5 kHz (Optech, 2009). The instrument has a 40° field of view in both the horizontal and vertical plane with a scanning range of 3 to 1700 m. For this survey, the ILRIS-3D was equipped with a pan-tilt base, providing a scanning field of 360° in the horizontal and 90° in the vertical. Each recorded point contains 5 items: Cartesian x, y, and z coordinate relative to the scanner's bolt hole reference point, normalized (0–255) backscatter intensity, and time (in s) since the scanner was powered on. In order to achieve an accurate time series of the lava lake, a pulse generator was used to time stamp each laser shot. The TLS was programmed to collect the last reflected pulse to minimize the number of returns recorded from the persistent gas and aerosol plume emitted from the lava lake.

The nominal one standard deviation range accuracy of the ILRIS-3D ER is 7 mm at 100 m (Optech, 2009). One significant contribution to error arises from the laser beam width, which increases as follows:

$$D_f = l \cdot \tan\theta + D_i \quad (1)$$

where D_i is the initial beam diameter (1.9 cm at 100 m), D_f is the final beam diameters, l is the scanning distance, and θ is the beam divergence angle (0.00974°; Petrie and Toth, 2008; Abellán et al., 2011). The actual position of the measured reflection can exist anywhere within the beam, meaning that the actual angular position of the measurement may be biased by up to half of the beam diameter (Pesci et al., 2011). This error is taken into account when reporting the spatial resolution of the instrument and depends on both the chosen sampling step and the laser beam width (Lichti and Jamtsho, 2006; Zhu et al., 2008; Pesci et al., 2011). This resolution measurement can aid in selecting the most appropriate sampling step (one that is at least two-thirds the size of the beam) while avoiding oversampling.

At Erebus, the rapidly varying quantity of volcanic gases within the optical path can have a significant effect on the range measurement. Other factors that may also contribute to the uncertainty of the TLS

data are pointing error (e.g., the vibration of the scanner (due in part to wind), causing repeat shots to strike at slightly different positions on the target area) and the varying reflectivity of the surfaces (Boehler et al., 2003). These other sources of error are difficult to quantify so we assessed their cumulative impacts (the overall accuracy of our measurements) by examining 0.5 × 0.5 m inactive areas along the Main Crater and Inner Crater walls, which were scanned repeatedly over the total scanning period. The inactive areas were sections of the wall that met the following criteria: (1) relatively planar; (2) spanned different levels of intensity (in order to measure the error over different types of surfaces); and (3) relatively immobile (<10 cm movement) over the three years of scanning and immobile (<5 cm movement) within an individual field season's scans. The resulting *x*, *y* and *z* measurements were then extracted and the RMSE calculation was performed. Five locations were extracted and analyzed, two on the Inner Crater Wall and three on the Main Crater Wall. This analysis indicated errors of 4.0 cm in the *x*-direction, 3.3 cm in the *y*-direction, and 2.1 cm in the vertical.

All scans reported here were made from a fixed site (Scanning Position 1 in Fig. 1), approximately 300 m by line of sight from the lava lake. In 2008 scans of the lava lake were collected every 1.5 min over a 4-h-period, with a spatial resolution of 2.6 cm at the lava lake. In 2009 and 2010, we imaged the lava lake height every minute over a single 8 h period each year, with spatial resolutions of 3.1 cm at the lava lake. The crater was scanned in December 2010 over a period of a week, in which 14 scans were acquired. Scans were taken from two scanning positions (Scanning Positions 1 and 2 in Fig. 1) on opposite sides of the crater rim in order to capture most of the crater. The scans had a mean spatial resolution of 3.6 ± 1.5 cm and were collected with at least 10% (4°) overlap to reduce alignment errors (Bellian et al, 2005).

An Airborne Laser Scanning (ALS) survey was flown over the summit plateau of Erebus volcano in 2001, providing the first high-resolution Digital Elevation Model (DEM) of the summit area (Csatho et al., 2008). The DEM was computed using a grid size of 2 m × 2 m and had an estimated RMS_z error of ±0.49 m (calculated using 12 independent ground-based GPS measurements). The 2001 ALS survey was

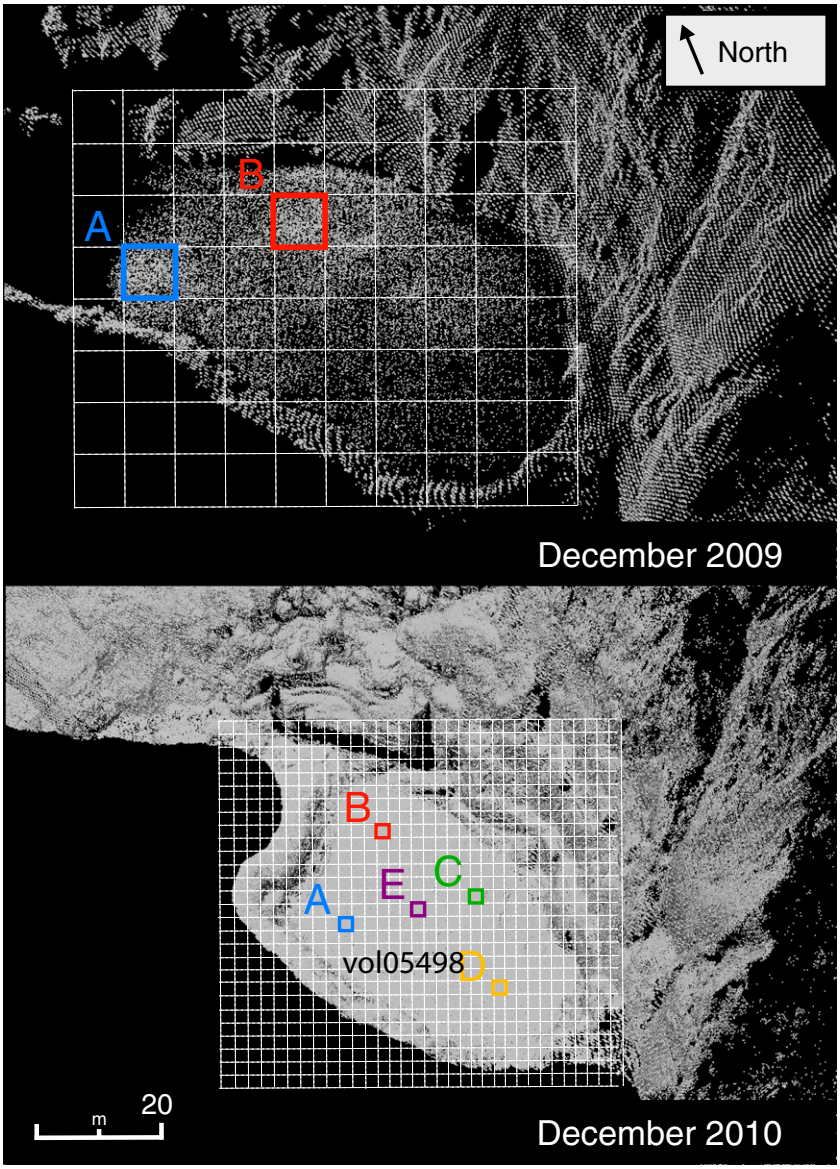

Fig. 2. Oblique TLS derived point clouds of the Erebus lava lake acquired on 15–16 December, 2009 (top) and 15 December, 2010 (bottom) at the same scale. The boxes correspond to the regions of interest (ROI) used to generate high-time resolution observations of surface elevation (Figs. 7 and 8). The 2009 ROIs cover areas of 8 m × 8 m while the 2010 ROIs consist of five 2 m × 2 m areas of the lake surface.

used to georeference all the TLS data, permitting assessment of decadal-scale changes in the summit crater.

3.2. Scan registration

All TLS and ALS point clouds were visualized, registered and analyzed using the PolyWorks v11.0 software (InnovMetric, 2010). Each TLS scan was collected in a unique scanner-centered coordinate system. To enable comparisons between scans, all the scans were transformed into a global coordinate system from the 2001 ALS data. No reference targets could be placed in the crater as access was impossible. Registrations were performed using the Best-Fit alignment tool in PolyWorks IMAlign. This uses an iterative algorithm, similar to the Iterative Closest Point algorithm described by Besl and McKay (1992), to minimize the 3-D distances between overlapping scans (e.g., Abellán et al., 2011). All scans collected during a single field season were registered to each other and then registered as a single rigid group to the previous year's data. The 2010 TLS scans were registered to the 2001 ALS DEM (Csatho et al, 2008), which provided a fixed reference. The surface-matching algorithm was only applied to parts of the crater that appeared to be stable between scans. Dynamic features such as the lava lake, blowing ice and dust, and areas affected by mass movements were manually excluded. Error associated with the alignment can be considered negligible, as Polyworks software resolves errors well beyond the total measurement error of the instrument.

The horizontal coordinates of the final aligned data are reported in WGS 84 (UTM zone 58S) and the elevations represent ellipsoid heights (WGS-84). The conversion from ellipsoid to orthometric heights can be easily preformed using open source calculators (e.g., see http://sps.unavco.org/geoid/). At Erebus volcano, the orthometric heights are about 54 m above the ellipsoid heights reported here.

3.3. Data extraction

The scans of the lava lake (from 2008, 2009 and 2010) were manually extracted from the point cloud and an average lava lake elevation and surface area were computed. Regions of interest (ROIs) of the lake were also isolated to examine differential elevation changes. The size and location of these ROIs were dictated by the density of the data and lake geometry and guided by our aim to quantify rapid (<10 min) changes across the lava lake surface (i.e., requiring a sufficiently short time step to characterize the rise and fall in level). This was hampered by the fluctuating plume opacity. All the points within the ROIs were collapsed into a 1-D elevation time series. The 2008 scans lacked sufficient data density to extract a time series of lake level height. The 2009 data were subdivided into 8 m × 8 m ROIs (Fig. 2); however only regions in the northern and the eastern section of the lake provided sufficiently dense data to extract a time series. The 2010 data, on the other hand, were both spatially and temporally well sampled, permitting extraction of five 2 m × 2 m ROIs (Fig. 2).

3.4. 3-D data visualization

In order to analyze and understand the morphology of the crater, it is essential to first create terrain classification maps using topographic attributes such as elevation and slope. To create such maps a Digital Elevation Model (DEM) of the crater was generated from the point cloud with a grid spacing of 0.25 m × 0.25 m. We also generated a DEM with a 2 m × 2 m grid spacing for compatibility with the 2001 ALS-derived model. A Triangulated Irregular Network (TIN) was also generated using the screened Poisson surface reconstruction method (Kazhdan and Hoppe, 2013) to create a true 3D visualization of the surface (Hutchinson and Gallant, 2000). The resolution of this generated surface is variable and directly depends on the density of the point cloud.

4. Results and analysis

4.1. Current morphology of the Main Crater

The generation of a DEM and TIN of the Main Crater from the 2010 TLS survey allowed for unprecedented accuracy (±0.25 m) in the visualization of features within the Main Crater (Fig. 3). The Main Crater rim is roughly elliptical with a 600 m NE oriented semi-major axes and a 470 m semi-minor axis. On the SW side of the Main Crater there is a terrace (referred to as the Main Crater floor), which has an area of 265 m^2 and lies an average of 135 m below the crater rim. The terrace has a mean slope of 14° and dips east towards the Inner Crater. The slope of the terrace decreases to 2° towards its center and increases up to 36° towards the Main Crater wall. The steep portion corresponds to a talus accumulation from rock falls down the Main Crater wall. Collapse events are also common along the Inner Crater wall, which cuts the terrace on

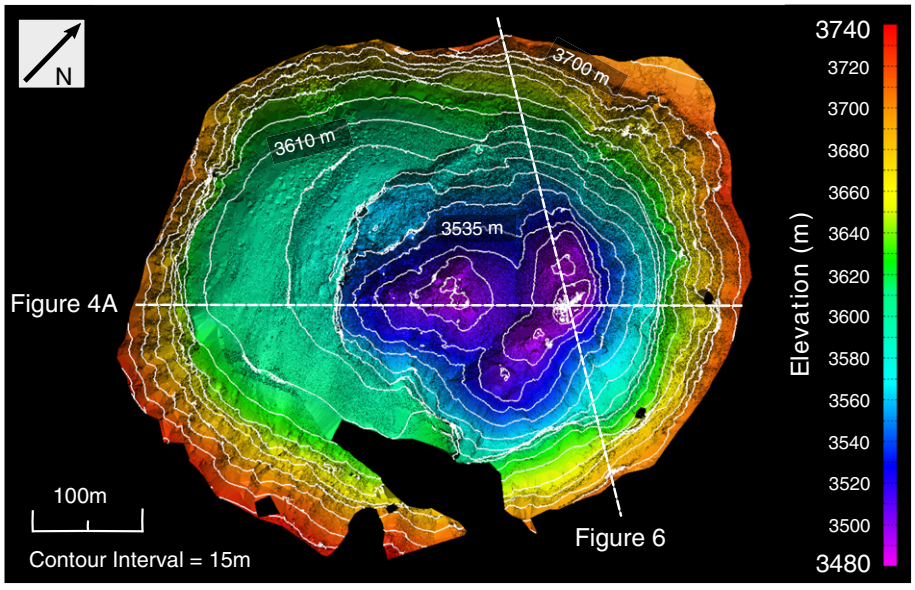

Fig. 3. Elevation contours overlain on the shaded relief map of the 0.25 m × 0.25 m DEM; transects refer to elevation profiles shown in Figs. 4a and 6. The elevations are ellipsoid heights (WGS-84).

its NE side. The entire NE edge of the terrace is cut by scarps. A significant collapse can be seen along the western edge of the Inner Crater wall; the collapsed material is significantly higher in elevation (at an average of 3558 m) than the surrounding Inner Crater floor (whose elevation ranges from about 3520 to 3540 m in that area). The 'Phreatic Crater' is a remnant of two major phreatic eruptions that occurred on 19 October 1993 and that widened the Inner Crater by 80 m to the SW (Dibble et al., 1994). This crater is no longer a prominent feature in the 2001 ALS survey (Csatho et al., 2008), likely due to the accumulation of wall collapse debris and infilling by lava bombs and spatter.

The Inner Crater, which is the focus of open-vent activity, is incised at the NE side of the Main Crater and its walls form a 320 m × 260 m diameter ellipse (elongated NE) (Fig. 3). In 2010 its deepest point was 75 m below the Main Crater floor and it hosts the active lava lake, several small active vents and numerous fumaroles (Figs. 3 and 4). The floor of the Inner has two depressions separated by an 80 m-wide spatter rampart (with a mean elevation of 3517 m; Fig. 4). The NE depression contains the main lava lake (sometimes referred to as Ray Lake in the literature) as well as three prominent fumaroles, while the SW depression hosts the "Werner Vent" (which has contained ephemeral lava lakes and lava flows, such as in the austral summers of 2004 and 2013) (Calkins et al., 2008). In 2010, the surface of the lava lake reached an average elevation of 3490 m and had an apparent surface area of 862 m^2. We note that the near edge of the lake is typically occluded from view from Scanning Position 1 by the spatter rampart above it, so computed lake areas should be regarded as minima (unless scans have been obtained from other suitable vantage points to obviate this problem).

4.2. Temporal changes of the Inner Crater and lava lake

4.2.1. Decadal-scale geomorphic change within the Inner Crater

We examined the morphological changes that occurred in the Main Crater over a decade by comparing the 2001 ALS survey to the 2010 TLS crater survey. This entailed subtracting the vertical coordinate of each grid cell in the 2001 ALS DEM from the equivalent grid cell vertical coordinate in the 2 m × 2 m 2010 TLS DEM (Fig. 5). The associated error is 0.52 m. The largest topographic changes are seen in the Inner Crater but minor elevation changes have also occurred along the Main Crater wall and floor that are associated with wall collapse events.

The floor of the NE depression within the Inner Crater was, on average, 23.7 m lower in 2010 compared with 2001 (Fig. 5). Vents on the floor subsided a mean 24.2 m and the lava lake surface was 27.1 m lower in 2010 than it was in 2001. The largest change, a lowering of 39.2 m on the SE side of the Inner Crater is associated with a collapse of the Main Crater wall and a widening of the depression zone by approximately 20 m. The Werner vent was 23.8 m lower in elevation in 2010. The collapse along the Inner Crater wall is clearly distinguished (Fig. 5) with an average drop in elevation of 26.4 m. A small area on the SW edge of the crater rose 5.3 m with accumulation of material and filling of the Phreatic Crater.

4.2.2. Annual changes in lava lake morphology

Annual TLS scans of the lava lake surface and the immediate surrounding areas allowed monitoring of the lava lake level, size and position within the Inner Crater (Table 1). When compared with the lava lake metrics derived from the 2001 ALS survey it again allows for a longer-term examination of changes in lake morphology. In 2001, the lava lake was elliptical with axes of 36 m and 21 m, and a surface area of 535 m^2. By 2008, the lake had more than tripled in size, with axial dimensions of 71 m × 38 m and a surface area of 1709 m^2. There was little change between 2008 and 2009 with just a 2 m decrease in the minor axis, and a negligible decrease in surface area to 1699 m^2. In 2010, the lava lake area halved to 862 m^2 with dimensions of 45 m × 26 m.

The location and elevation of the lava lake also varied from year-to-year. The average surface elevation of the lake was 3517 m in 2001, 3497 m in 2008, 3494 m in 2009 and 3490 m in 2010 (Fig. 6). While there is a significant gap in observations between 2001 and 2008, the measurements are consistent with a 3 m per year fall in lake level. Over the 2 year TLS study period from 2008 to 2010 the lake level was 7 m lower consistent with the overall 3 m per year trend from 2001 to 2008. We also find that the midpoint of the lava lake migrated 24 m to the SE over this period (see Table 1 and Fig. 6).

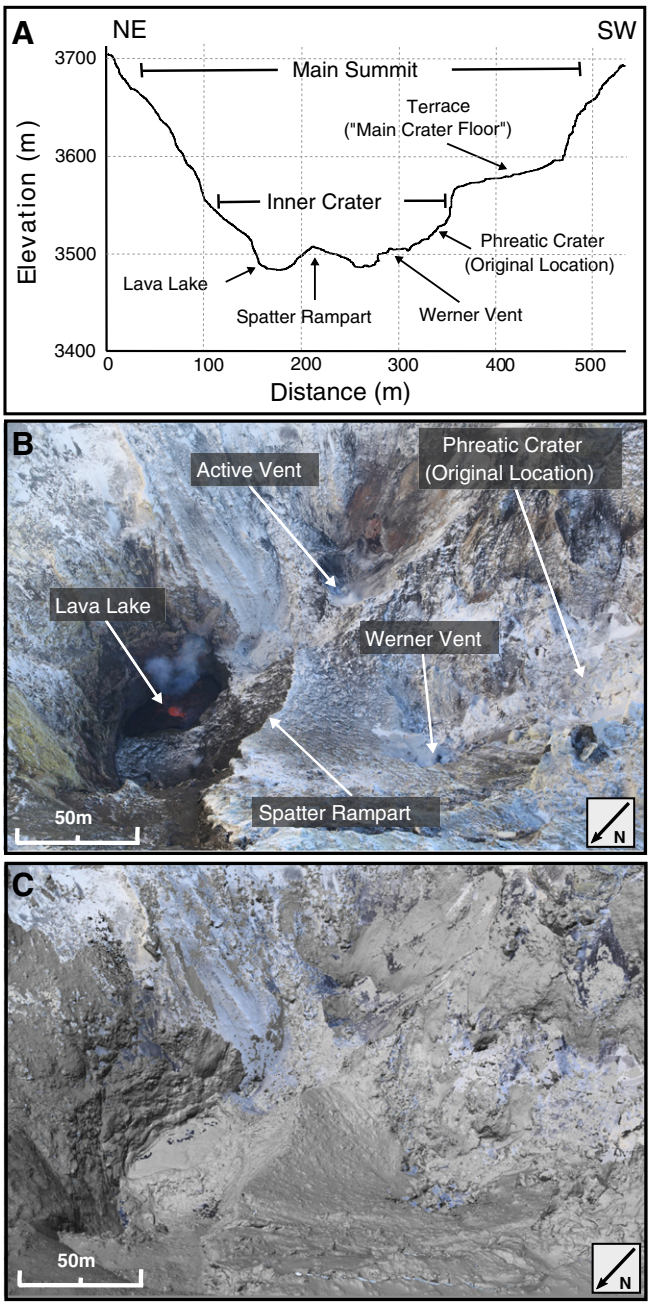

Fig. 4. (A) Elevation profile across the Main Summit Crater showing the main morphological features within the Inner Crater. (B) Photograph of the Inner Crater taken in December 2010 from Scanning Position 1 (Fig. 1), with principal features identified; (C) the TLS point cloud of the Inner Crater in December 2010.

4.3. Time series of lava lake surface elevation

Variations in the lava lake elevations were made over 151 min on 15/16 December 2009 and for 350 min on 15 December 2010 (350 min). The time series clearly identify cyclic changes in lava lake level (Figs. 7 and 8).

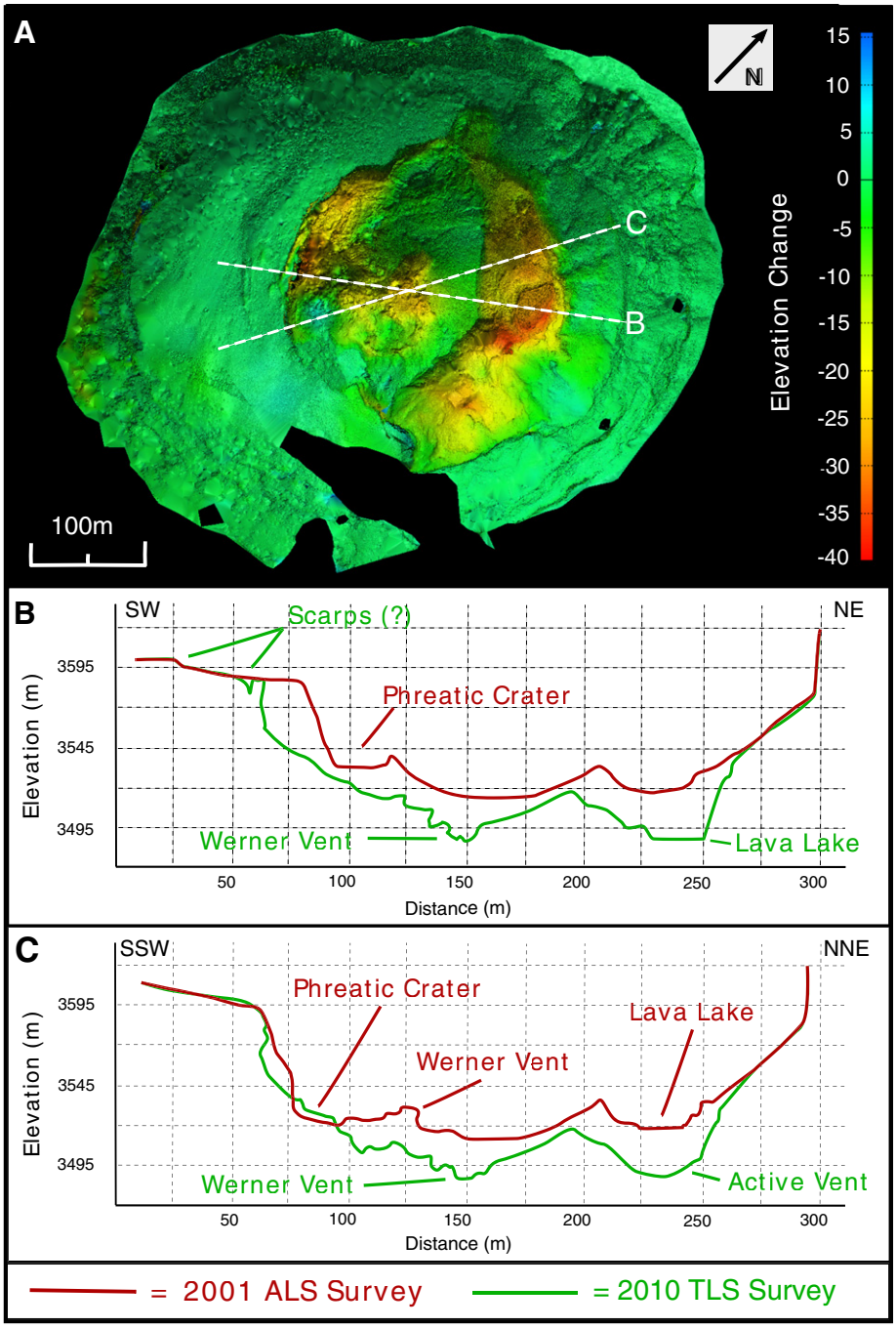

Fig. 5. (A) Map of elevation changes that occurred between the 2001 ALS survey and the 2010 TLS survey, overlain on the shaded relief map of the 0.25 m × 0.25 m DEM; dashed lines refer to (B) SW–NE and (C) SSW–NNE transects across the Inner Crater showing elevation profiles for both the 2001 and 2010 datasets, with major feature identified. Note the significant changes in elevation that occurred over this time interval — including a general lowering of elevations within the Inner Crater (focused close to the lava lake and assorted vents), and erosion of the western Inner Crater wall and "Phreatic Crater." The elevations are ellipsoid heights (WGS-84).

4.3.1. December 2009

For the 2009 data, two ROIs approximately 30 m apart were used to derive time series of lake levels (Fig. 7a). The two time series appear synchronous at the temporal resolution of the scans and we cannot identify any clear or consistent leads or lags between them. Minor differences in amplitude characterize the two ROIs, with elevations at ROI "B" averaging 0.2 m lower than those of ROI "A". Periods of cycles ranged from 8 to 21 min with an average of 16.2 ± 4.1 (1σ) min. The largest change in surface elevation we observed was a rise of about 1.5 m (representing a volume increase of 2550 m^3 in the lava lake; Fig. 7b) over a period of 12 min. The average change in surface elevation (amplitude) per cycle was 0.91 ± 0.34 (1σ) m.

Taking the first derivatives of lake level and lake volume yields plots of vertical rise/fall rate of the lake surface (Fig. 7c) and rate of volumetric change (Fig. 7d). These indicate comparable vertical rise and fall rates of the lake, from 0.2 to 0.4 cm s^{-1}. These speeds are an order of magnitude slower than the horizontal motion of the lake surface (Peters et al., 2014b). Similarly, volumetric rates of change are typically 2–7 m^3 s^{-1} (mean of 3.2 ± 0.6 m^3 s^{-1} for rising lake levels and 3.9 ± 1.4 m^3 s^{-1} for falling levels).

Table 1
A summary of lava lake characteristics for each year of lidar survey (ALS and TLS). Elevations in ellipsoid heights (WGS-84).

Year	Max length (m)	Max width (m)	Surface area (m^2)	Lava lake center coordinates		
				UTM Southing (m)	UTM Easting (m)	Elevation (m)
2001	36	21	535	1,393,469	552,181	3517
2008	71	38	1709	1,393,468	552,191	3497
2009	71	36	1699	1,393,466	552,192	3494
2010	45	26	862	1,393,458	552,202	3490

4.3.2. December 2010

For the 2010 case, five ROIs on the lake surface were selected approximately 10–20 m apart (Figs. 2 and 8). The cyclic rise and fall in lake level is evident through most of the record, with amplitude averaging around 0.65 m. This is somewhat less than for the 2009 oscillations, although the brevity of the observation periods precludes drawing too much from this difference. The 2010 dataset exhibits greater variation but it is of longer duration and spans a number of degassing events. The mean cycle period is 12 min, ranging from 4 to 18 min. Despite some differences in amplitude and absolute levels between the different ROIs, the trends appear synchronous. Some consistent topographic differences emerge when comparing the ROIs: elevations extracted for ROI "C" are ~0.15 m above the lake average, whereas those for ROI "D" ~0.3 m below the average. Elevations for the centrally-positioned ROI "E", for which there are far more dense data, tend to lie intermediate to the more peripheral ROIs. Volumetric changes were 1.8 ± 0.8 m^3 s^{-1} for rising lake levels, and 1.9 ± 1.0 m^3 s^{-1} for falling lake levels. These are significantly different from the preceding year and may reflect the decreased lava lake area (862 m^3) compared with 2009 (1699 m^3).

4.3.3. Eruptions on 15 December 2010

A striking feature in the 15 December 2010 time series is the abrupt emptying and rapid refilling of the lake during a minor bubble burst explosion at 03:38 UTC (Fig. 8a). The eruption ejected lava bombs across the Inner Crater. The lake level dropped an average of 3.23 m within the 1 min time-step, corresponding to an ~2780 m^3 volume change in the lake. Over the next 6 min, the lake steadily refilled to the level maintained in the hour preceding the eruption. At this time, a large bubble approached the lake surface (corroborated visually) associated with a further 1.1 m surface lift over the next 4 min. The 5–10 m diameter bubble burst at 03:52 UTC, releasing a plume of gas and aerosol, and preceding deflation of the lake surface by ~1.7 m over the next 8 min. This pattern was repeated following about 1.5 m level rise over the next 55 min, another bubble burst at 04:34 h with subsequent 1.61 m deflation (over 9 min).

The more rapid volume changes are associated with a drop in lava lake following the bubble burst events. The largest at 03:38 (Fig. 8) decreased lake volume at a rate of over 40 m^3 s^{-1}. This value represents a minimum since it is time-averaged over the 49 s scan period. The subsequent volumetric rate of recharge exceeded 6 m^3 s^{-1} (i.e., more than three times the typical rates associated with cyclic behavior). The ensuing bubble bursts decreased the lava volume at a rate of ~4 m^3 s^{-1}; it then refilled at ~2–3 m^3 s^{-1}.

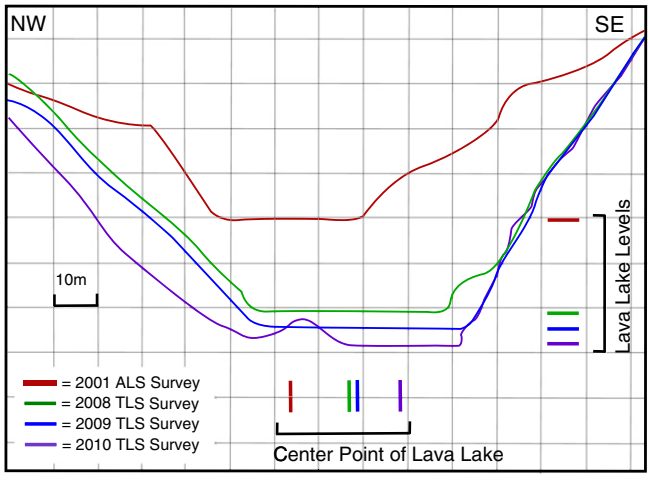

Fig. 6. Extracted surface elevations for lava lake profiles shown in Fig. 3, for the multi-year collections of TLS point clouds with the 2001 ALS profile also shown. The profiles suggest a progressive fall in lake level of ~3 m a^{-1} over this time interval. Lines have been drawn through the point clouds to aid visualization of the mean surface and levels. The scatter within the annual profiles reflects the cyclic rise and fall in lake level (Figs. 7 and 8), and the larger variation in level seen in the 2010 point cloud data reflects an explosive bubble burst that partially evacuated the lava lake during acquisition.

5. Discussion

5.1. Geomorphology of the Erebus summit region

Comparison of the 2010 TLS and 2001 ALS surveys provides the first quantitative observations of geomorphic changes within the Erebus summit crater. The minimal changes apparent on the flanks of the summit crater are consistent with previous studies (Otway et al., 1994; Murray et al., 2006), which identified little to no deformation in these areas. The subsidence we observed was confined to the Inner Crater floor with the largest subsidence focused around the lava lake and fumarolic vents (Fig. 5). The sub-circular pattern of deformation is suggestive of a ring fault system (Gudmundsson, 2007; Holohan et al., 2011) whose surface expression defines the extent of the Inner Crater. The current subsidence is accommodated by slip along these curved faults and fractures and leads to the development of steep and in some cases overhanging walls prone to collapse (Pavez et al., 2006). These wall collapse events have been observed on Erebus for over 50 years, and combined with the evidence for changes in the Inner Crater suggest sustained (continuous or episodic) deformation (Fig. 9).

The changes observed within the Main Crater can be attributed to a combination of gravitational failure of steep surfaces and endogenous magmatic processes. The circular pattern of subsidence (forming the Inner Crater) is consistent with the deflation of a near-surface magma body (Pavez et al., 2006; Gudmundsson, 2012). Seismological evidence, however, has suggested that the shallow magma reservoir at Erebus is located roughly 500 m WNW of the Main Crater (Aster et al., 2003, 2008; Zandomeneghi et al., 2013), eliminating it as a candidate source responsible for the observed deformation. It is possible that an additional near-surface magma body or bodies exists beneath the Inner Crater. A complex near-surface magma system would also explain the spatial distribution of deformation, i.e., the small-scale differences evident across the Inner Crater floor.

5.2. Cyclic behavior of the lava lake

Several inferences have been made based on observed gas emissions from the lake (Ilanko et al., 2015) and lake surface motion studies (Peters et al., 2014a,b). These are that the lava lake is likely highly permeable and that the cyclic behavior arises from episodic flow of degassing magma into the lake. This may be due to unsteadiness in the viscous exchange flow in the subjacent conduit (Oppenheimer et al., 2009). Here, we consider two aspects of our observations to shed further light on the remarkable behavior of the lava lake. The first is the lack of evidence for obvious time lags in the spatial pattern of lake level rise and fall. While we do observe a few tens of cm of topographic variation in the lake surface elevation at an instant in time (which likely reflect the surface roughness of the lava and the presence of flow lobes), the surface as a whole exhibits a piston-like vertical motion. It is not obvious, for instance, that lava wells up in the center of

the lake and migrates across the surface to the periphery. Rather it seems the whole surface is lifted up and subsequently deflates simultaneously. This suggests the rapid establishment of magmastatic equilibrium of the lake level in response to the processes driving the oscillations.

A key observation we note is the synchroneity of the recorded lake cycles with our height and spatial analysis. As noted, Peters et al. (2014a) recognized that the high stand of the lava lake preceded the otherwise synchronous peaks in lake surface speed (in the horizontal plane), SO_2 flux and, oxygen fugacity (fO_2) of the emitted gases. However, we have shown that the rate of volume increase of the lake reaches a peak about 5 min before the maximum level is achieved (Figs. 7 and 8). This suggests that cycles are fundamentally driven by episodic changes in the gas volume fraction within the magma column, an explanation used to interpret fluctuating levels in "lake" level in an experimental model by Witham et al. (2006). There is a delay between the ascent of a pulse of vesiculating magma in the upper region of the conduit and the emission of the associated gas from the lake surface that reflects the permeability of the lake–conduit system. Recent gravity observations at Kīlauea volcano, Hawai'i, have highlighted the high porosity of the basaltic lava lake at Halema'uma'u (Carbone et al., 2013). In this case, the periods of cycles are presumably a function of unsteady dynamics of the viscous exchange flow expected to prevail in the conduit feeding the lava lake (e.g., see Beckett et al., 2014, though note that this work relates to the basaltic magma plumbing of Stromboli volcano).

Over the three years of our study, the net magma flux to the Erebus lava lake was zero. The typical rates of volumetric change in the lava lake associated with both rising and falling levels are approximately 2–4 $m^3\ s^{-1}$. In contrast, the mean flux of gas out of the lake through a cycle is around 20 $m^3\ s^{-1}$ (Peters et al., 2014b). Lake level may rise as

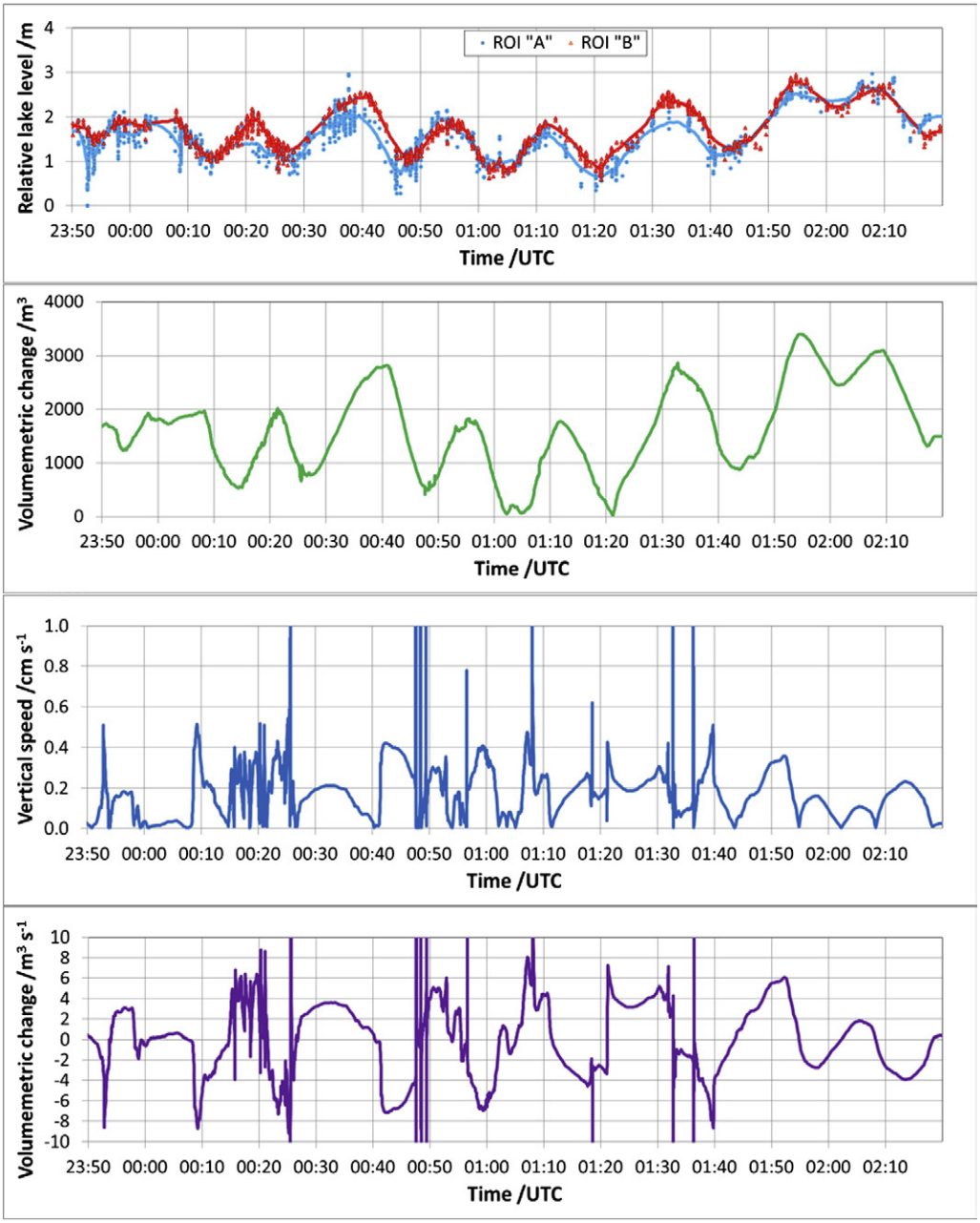

Fig. 7. Time series of December 2009 lava lake surface elevations for ROIs A and B in Fig. 2 and measurements extracted from TLS observations starting 23:50 on 15 December UTC and ending 02:20 16 December UTC (local time is UTC + 13 h). (a) Relative lake surface level for the two ROIs. Raw data are shown as symbols and the running average shown in solid lines. (b) Relative volume change in the lava lake computed for ROI "B" and using the calculated lake area (1699 m^2; Table 1). (c) Absolute vertical rise and fall speed of the lava lake computed from first derivative of elevation time series in (a) for ROI "B". (d) Relative rate of volumetric change computed from first derivative of time series in (c).

an ascending pulse of magma vesiculates in the conduit (pushing overlying degassed magma back into the lake) and as the degassing pulse enters the lake. The timescale of gas release at the surface will be a function of the length scales involved and the permeability of lava and its interfaces with the host rock. The peak rise speed of the lake surface may correspond to entry of the degassing pulse into the lake, whose depth appears to be a few tens of meters. Shortly after the peak in lake level, the magma pulse reaches the surface, and flow speeds in the horizontal plane reach a maximum as they spread gravitationally across the surface. The gas flux out of the lake reaches its peak, and its chemical signature corresponds to the redox conditions of the magma pulse. At this time, the volume of the lake is already decreasing through a combination of decreasing gas volume fraction and drainage of dense magma back into the conduit. The cycle repeats as the next pulse of degassing magma approaches the top of the conduit.

The flux of magma required to supply the observed gas emission is difficult to constrain. One approach is to take the typical flux of H_2O in the gas plume emitted from the lava lake (around 10 kg s^{-1};

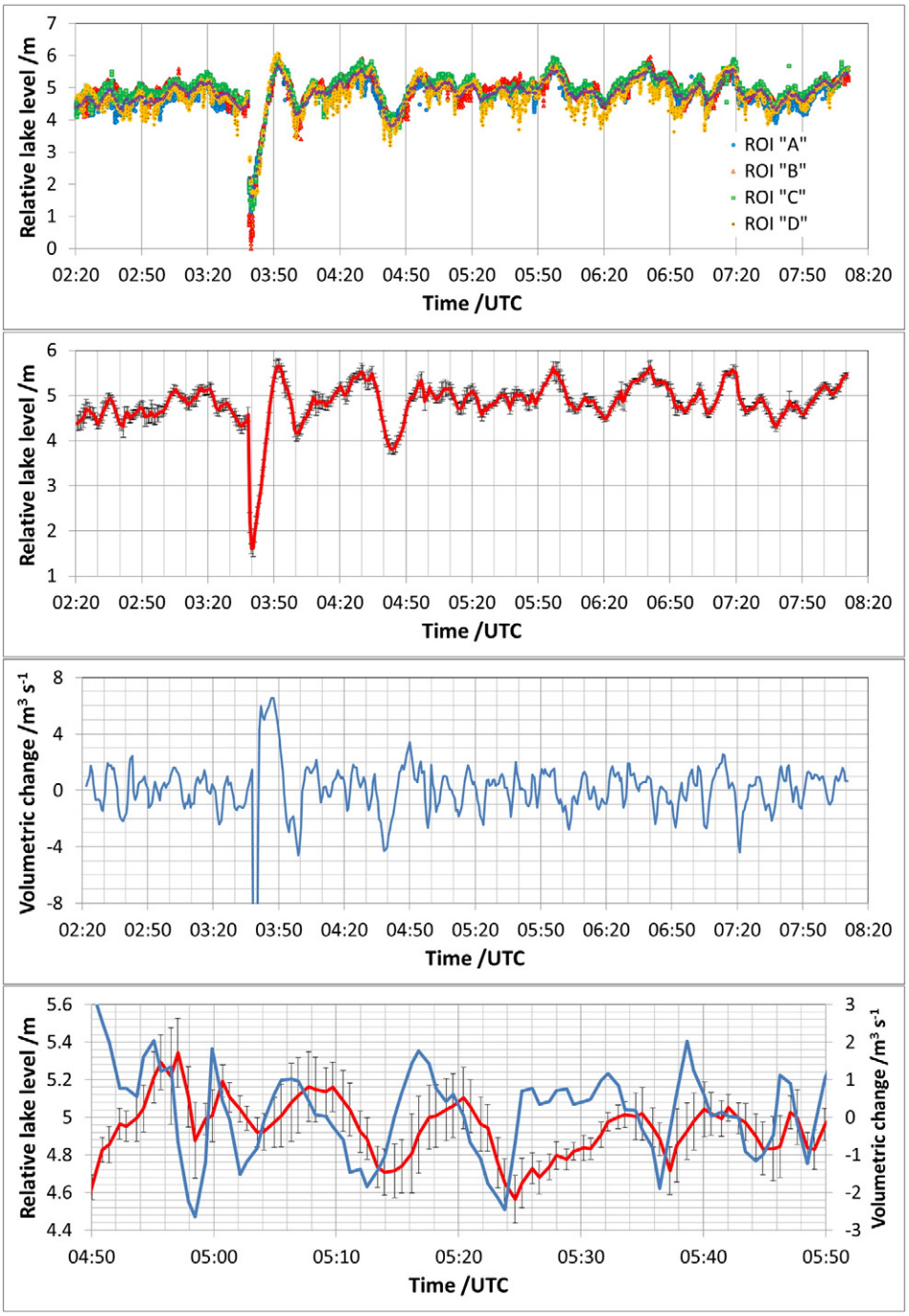

Fig. 8. Time series of lava lake surface elevations for ROIs A–E in Fig. 2b and derived measurements, extracted from TLS observations acquired on 15 December 2010 (UTC). (a) Relative lake surface level for the five ROIs with raw data shown as symbols and running average shown in solid traces, except for ROI "E" in the center of the lake for which there are sufficient data to compute the mean level per TLS scan. Note the sudden partial emptying of the lake accompanying the rupture of a large gas bubble at the lake surface at 03:38 h. (b) Relative lake surface level for ROI "E" with intra-scan level variation represented by $\pm 1\sigma$ error bars. (c) Relative rate of volume change in the lava lake computed for ROI "E" and using the calculated lake area (862 m^2; Table 1). (d) Zoom-in of a 1 h interval of the time series juxtaposing the relative lake level and rate of volume change. Note how taking the first derivative of the lake level data indicates that maximum volumetric changes (blue) occur before the peak surface lake level (red) is reached.

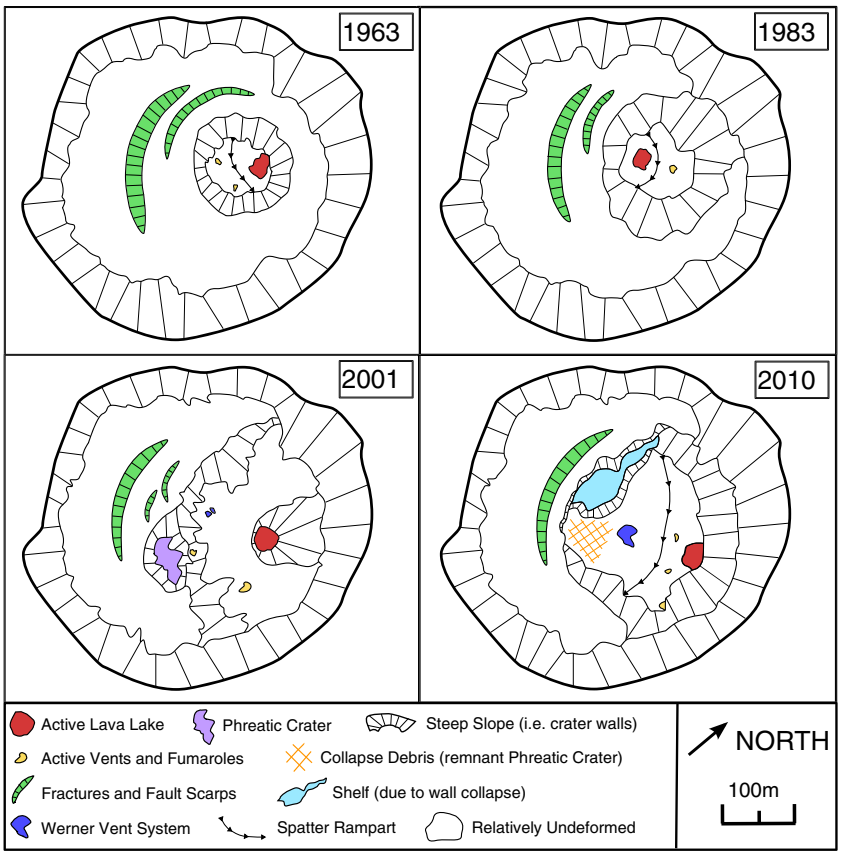

Fig. 9. Schematic maps of the Main Crater for 1963, 1983, 2001 and 2010 illustrating the principal changes that have occurred over the last half century.
Based on aerial photographs and data reported by Lyon and Giggenbach (1974), Kyle and McIntosh (1978), Kyle et al. (1982), Blick et al. (1989) and Csatho et al. (2008) and our TLS surveys.

Oppenheimer and Kyle, 2008) and the estimated water content of Erebus phonolite (up to 0.2 wt.%; Moussallam et al., 2013). Accounting for crystal volume fractions, this would correspond to a dense magma volume flux of order 2.7 $m^3\ s^{-1}$. This is surprisingly close to the typical rates of volume change in the lava lake but we consider this to be coincidental given the likely greater significance of variable gas volume fraction. However, this value permits us to consider magma ascent rates in the conduit. For a conduit of radius 3.5 m (Oppenheimer et al., 2009), the ascent rate (as dense magma) is around 7 cm s^{-1} (comparable to maximum lava flow rates across the surface of the lake; Peters et al., 2014b). In half a lake cycle (circa 6 min), this would amount to a magma ascent of approximately 25 m. For the 2010 lake area (862 m^2), injecting 25 m of conduit magma into the lava lake would represent about 1 m of surface lift. These simple calculations lend some support to the hypothesis that the lava lake rise and fall cycles are driven by episodic arrival of degassing magma pulses at the top of the conduit.

5.3. The lava lake's response to explosions

We were fortunate to capture the lake surface level change associated with a minor explosion at 03:38 on 15 December 2010. The drop in lake level of more than 3 m represents an impulsive disturbance of the magmastatic equilibrium to which the system rapidly responds. The refilling of the lake and rise in elevation took place over the next 6 min with a volumetric recharge rate of around 6 $m^3\ s^{-1}$ (Fig. 8c). This is greater than the rate of change associated with the cyclic lake level rise by a factor of three or so. This is substantially less than the change in flow rate that might be expected for a switch from bi-directional to un-directional flow, which would be of order 16 (based on a doubling of flow radius, r, and proportionality of flow rate to r^4; according to modified versions of the Poiseuille equation e.g., Stevenson and Blake, 1998).

6. Concluding remarks

We have demonstrated the application of Terrestrial Laser Scanning to measurements of the complex spatial–temporal changes occurring in the summit crater of Erebus volcano. Changes range from the geomorphic scale of ground deformation and slope processes occurring in the Inner Crater between field seasons to the temporal and spatial scales of the fluid dynamics of the lava lake and its feeder conduit. Using these measurements we have been able to quantify rates of surface rise and fall and associated volumetric changes in the lake, which provide new constraints on the dynamics of the conduit and its associated plumbing system.

Operation of the TLS does require uncommonly favorable conditions at the summit of Erebus, notably in respect of relative humidity, which dictates the opacity of the plume. High humidity days and the associated reduction in visibility within the crater prevent collection of useful TLS observations. Nevertheless, the flexibility of the technique in respect of controlling scan time step and target area, and the accuracy and precision of the range data offer unprecedented insights into the crater geomorphology and characteristics of the lava lake. These would be extremely difficult to quantify by alternative means, especially in view of the inaccessibility of the crater. Future work could include collection of extended data sets of the lava lake height and its spatial variation coincident with spectroscopic gas chemistry and flux measurements.

Acknowledgments

This material is based upon work supported by the National Science Foundation (Division of Polar Programs) under Grants ANT0838817 and ANT1142083. The Optech ILRIS 3D TLS instrument was provided by the UNAVCO Polar group with support from NSF grant award ANT0723223. CO receives additional support from the NEC Centre for the Observation and Modeling of Earthquakes, volcanoes and Tectonics (COMET). We gratefully acknowledge the following for assisting with fieldwork on Erebus: Nelia Dunbar, Bill McIntosh, Aaron Curtis, Nels Iverson, Matt Zimmerer, Melissa Kammerer, Nial Peters, Kayla Iacovino, Yves Moussallam, Tehnuka Ilanko, Anna Barford, and Harry Keys. We also acknowledge tremendous logistical support from the staff and the civilian contractors working out of McMurdo station on behalf of the Division of Polar Programs of NSF. We extend especial thanks to the helicopter support provided by PHI and Helicopters, New Zealand. We thank Mark Murray and Rick Aster for their comments on an early version of the manuscript, and Carolyn Parcheta and anonymous for formal reviews of the submitted manuscript.

References

Abellán, A., Vilaplana, J.M., Calvet, J., Garcia-Sellés, D., Asensio, E., 2011. Rockfall monitoring by Terrestrial Laser Scanning — case study of the basaltic rock face at Castellfollit de la Roca (Catalonia, Spain). Nat. Hazards Earth Syst. Sci. 11, 829–841. http://dx.doi.org/10.5194/nhess-11-829-2011.

Aletti, M., Burgisser, A., Scaillet, B., Oppenheimer, C., 2014. Chloride partitioning and solubility in hydrous phonolites from Erebus volcano: a contribution towards a multicomponent degassing model. GeoResJ 3–4, 27–45. http://dx.doi.org/10.1016/j.grj.2014.09.003.

Aster, R., Mah, S., Kyle, P., McIntosh, W., Dunbar, N., Johnson, J., Ruiz, M., McNamara, S., 2003. Very long period oscillations of Mount Erebus volcano. J. Geophys. Res. 108, 2522. http://dx.doi.org/10.1029/2002JB002101.

Aster, R., Zandomeneghi, D., Mah, S., McNamara, S., Hendersono, D.B., Knox, H., Jones, K., 2008. Moment tensor inversion of very long period seismic signals from Strombolian eruptions of Erebus Volcano. J. Volcanol. Geotherm. Res. 177, 635–647. http://dx.doi.org/10.1016/j.jvolgeores.2008.08.013.

Beckett, F.M., Burton, M., Mader, H.M., Phillips, J.C., Poland, M., Rust, A.C., Whitham, F., 2014. Conduit convection driving persistent degassing at basaltic volcanoes. J. Volcanol. Geotherm. Res. 283, 19–35. http://dx.doi.org/10.1016/j.jvolgeores.2014.06.006.

Bellian, J.A., Kerans, C., Jennette, D.C., 2005. Digital outcrop models: applications of terrestrial scanning lidar technology in stratigraphic modeling. J. Sediment. Res. 75, 166–176.

Besl, P.J., McKay, N.D., 1992. A method for registration of 3-D shapes. IEEE Trans. PRMI 14, 239–255. http://dx.doi.org/10.1109/34.12.1791.

Blick, G.H., Otway, P.M., Scott, B.J., 1989. Deformation monitoring of Mt. Erebus, Antarctica, 1980–1985. In: Latter, J.H. (Ed.), Volcanic Hazards. IAVCEI Proceedings in Volcanology vol. 1. Springer, Berlin Heidelberg, pp. 554–560. http://dx.doi.org/10.1007/978-3-642-73759-6_32.

Boehler, W., Vincent, M.B., Marbs, A., 2003. Investigating laser scanner accuracy. Int. Arch. Photogramm. Remote. Sens. Spat. Inf. Sci. 34 (5), 696–701.

Boichu, M., Oppenheimer, C., Tsanev, V., Kyle, P.R., 2010. High temporal resolution SO_2 flux measurements at Erebus volcano, Antarctica. J. Volcanol. Geotherm. 190 (3), 325–336. http://dx.doi.org/10.1016/j.jvolgeores.2009.11.020.

Burgisser, A., Oppenheimer, C., Alletti, M., Kyle, P.R., Scaillet, B., Carroll, M.R., 2012. Backward tracking of gas chemistry measurements at Erebus volcano. Geochem. Geophys. Geosyst. 13, Q11010. http://dx.doi.org/10.1029/2012GC004243.

Calkins, J., Oppenheimer, C., Kyle, P., 2008. Ground-based thermal imaging of lava lakes at Erebus volcano, Antarctica in December 2004. J. Volcanol. Geotherm. Res. 177, 695–704. http://dx.doi.org/10.1016/j.jvolgeores.2008.02.002.

Carbone, D., Poland, M., Patrick, M., Orr, T., 2013. Continuous gravity measurements reveal a low-density lava lake at Kilauea Volcano, Hawai'i. Earth Planet. Sci. Lett. 376, 178–185.

Cashman, K.V., Soule, S.A., Mackey, B.H., Deligne, N.I., Deardorff, N.D., Dietterich, H.R., 2013. How lava flows: new insights from applications of lidar technologies to lava flow studies. Geosphere 9 (6), 1664–1680.

Csatho, B., Schenk, T., Kyle, P., Wilson, T., Krabill, W.B., 2008. Airborne laser swath mapping of the summit of Erebus volcano, Antarctica: applications to geological mapping of a volcano. J. Volcanol. Geotherm. Res. 177, 531–548. http://dx.doi.org/10.1016/j.jvolgeores.2008.08.016.

Dibble, R.R., Kyle, P.R., Skov, M., 1994. Volcanic activity and seismicity of Mount Erebus, 1986–1994. Antarct. J. U. S. 29, 11–14.

Dibble, R.R., Kyle, P.R., Rowe, C.A., 2008. Video and seismic observations of Strombolian eruptions at Erebus volcano, Antarctica. J. Volcanol. Geotherm. Res. 177, 619–634.

Esser, R.P., Kyle, P.R., McIntosh, W.C., 2004. $^{40}Ar/^{39}Ar$ dating of the eruptive history of Mount Erebus, Antarctica: volcano evolution. Bull. Volcanol. 66, 671–686. http://dx.doi.org/10.1007/s00445-004-0354-x.

Gudmundsson, A., 2007. Conceptual and numerical models of ring-fault formation. J. Volcanol. Geotherm. Res. 116, 142–160. http://dx.doi.org/10.1016/j.jvolgeores.2007.04.018.

Gudmundsson, A., 2012. Magma chambers: formation, local stresses, excess pressures, and compartments. J. Volcanol. Geotherm. Res. 237–238, 19–41. http://dx.doi.org/10.1016/j.jvolgeores.2012.05.

Harpel, C.J., Kyle, P.R., Esser, R.P., McIntosh, W.C., Caldwell, D.A., 2004. $^{40}Ar/^{39}Ar$ dating of the eruptive history of Mount Erebus, Antarctica: summit flows, tephra, and caldera collapse. Bull. Volcanol. 66, 687–702. http://dx.doi.org/10.1007/s00445-004-0349-7.

Holohan, E.P., Schöpfer, M.P.J., Walsh, J.J., 2011. Mechanical and geometric controls on the structural evolution of pit crater and caldera subsidence. J. Geophys. Res. 116, B07202. http://dx.doi.org/10.1029/2010jb00803.

Hutchinson, M.F., Gallant, J.C., 2000. Digital elevation models and representation of terrain shape. In: Wilson, J.P., Gallant, J.C. (Eds.), Terrain Analysis: Principles and Applications. Wiley, New York, pp. 29–50 (Chapter 2).

Ilanko, T., Oppenheimer, C., Burgisser, A., Kyle, P., 2015w. Cyclic degassing of Erebus volcano, Antarctica. Bull. Volcanol. (in revision).

InnovMetric, Inc., 2010. Polyworks v11.0. www.innovmetric.com.

James, M.R., Pinkerton, H., Applegarth, L.J., 2009. Detecting the development of active lava flow fields with a very-long-range terrestrial laser scanner and thermal imagery. Geophys. Res. Lett. 36, L22305. http://dx.doi.org/10.1029/2009GL040701.

Kazhdan, M., Hoppe, H., 2013. Screened Poisson surface reconstruction. ACM Trans. Graph. 32 (3). http://dx.doi.org/10.1145/2487228.2487237 (Article 29, June).

Kelly, P.J., Dunbar, N.W., Kyle, P.R., McIntosh, W.C., 2008. Refinement of the late Quaternary geologic history of Erebus volcano, Antarctica using $^{40}Ar/^{39}Ar$ and ^{36}Cl age determinations. J. Volcanol. Geotherm. Res. 177, 569–577.

Kyle, P.R., McIntosh, W., 1978. Observations of volcanic activity at Mt. Erebus, 1978. Antarct. J. U. S. 13, 32–34.

Kyle, P.R., Dibble, R.R., Giggenbach, W.F., Keys, J., 1982. Volcanic activity associated with the anorthoclase phonolite lava lake, Mt. Erebus, Antarctica. In: Craddock, C. (Ed.), Antarctic Geosciences. University of Wisconsin Press, pp. 735–745.

Kyle, P.R., Moore, J.A., Thirlwall, M.F., 1992. Petrologic evolution of anorthoclase phonolite lavas at Mount Erebus, Ross Island, Antarctica. J. Petrol. 33, 849–875. http://dx.doi.org/10.1093/petrology/33.4.849.

Kyle, P.R., Sybeldon, L.M., McIntosh, W.C., Meeker, K., 1994. Sulfur dioxide emission rates from Mount Erebus, Antarctica. In: Kyle, P.R. (Ed.), Volcanological and Environmental Studies of Mount Erebus, Antarctica. Antarctic Research Series 66, pp. 69–82.

Le Losq, C., Neuville, D.R., Moretti, R., Kyle, P.R., Oppenheimer, C., 2015. Rheology of phonolite magmas — the case of the Erebus lava lake. Earth Planet. Sci. Lett. 411, 53–61.

Lichti, D.D., Jamtsho, S., 2006. Angular resolution of terrestrial laser scanners. Photogramm. Rec. 21, 141–160. http://dx.doi.org/10.1111/j.1477-9730.2006.00367.x.

Lyon, G.L., Giggenbach, W.F., 1974. Geothermal activity in Victoria Land, Antarctica, New Zealand. J. Geol. Geophys. 17, 511–521. http://dx.doi.org/10.1080/00288306.1973.10421578.

Moussallam, Y., Oppenheimer, C., Scaillet, B., Kyle, P., 2013. Experimental phase-equilibrium constraints on the phonolite magmatic system of Erebus volcano, Antarctica. J. Petrol. 54, 1285–1307. http://dx.doi.org/10.1093/petrology/egt012.

Moussallam, Y., Oppenheimer, C., Scaillet, B., Gaillard, F., Kyle, P., Peters, N., Hartley, M., Berlo, K., Donovan, A., 2014. Tracking the changing oxidation state of Erebus magmas, from mantle to surface, driven by magma ascent and degassing. Earth Planet. Sci. Lett. 393, 200–209. http://dx.doi.org/10.1016/j.epsl.2014.02.055.

Murray, M.H., Kyle, P.R., Aster, R.C., Bartel, B., 2006. Continuous GPS measurement of deformation at Erebus Volcano, Antarctica. AGU Fall Mtg Abstract.

Nelson, C.E., Jerram, D.A., Hobbs, R.W., Terrington, R., Kessler, H., 2011. Reconstructing flood basalt lava flows in three dimensions using terrestrial laser scanning. Geosphere 7 (1), 87–96.

Nguyen, H.T., Fernandez-Steeger, T.M., Wiatr, T., Rodrigues, D., Azzam, R., 2011. Use of terrestrial laser scanning for engineering geological applications on volcanic rock slopes—an example from Madeira Island (Portugal). Nat. Hazards Earth Syst. Sci. 11, 807–817.

Nield, J.M., Chiverrell, R.C., Darby, S.E., Leyland, J., Vircavs, L.H., Jacobs, B., 2013. Complex spatial feedbacks of tephra redistribution, ice melt and surface roughness modulate ablation on tephra covered glaciers. Earth Surf. Process. Landf. 38 (1), 95–102.

Norini, G., Acocella, V., 2011. Analogue modeling of flank instability at Mount Etna: understanding the driving factors. J. Geophys. Res. 116. http://dx.doi.org/10.1029/2011JB008216.

Oppenheimer, C., Kyle, P.R., 2008. Probing the magma plumbing of Erebus volcano, Antarctica, by open-path FTIR spectroscopy of gas emissions. J. Volcanol. Geotherm. Res. 177 (3), 743–754.

Oppenheimer, C., Lomakina, A.S., Kyle, P.R., Kingsbury, N.G., Boichu, M., 2009. Pulsatory magma supply to a phonolite lava lake. Earth Planet. Sci. Lett. 199, 173–184. http://dx.doi.org/10.1016/j.epsl.2009.04.043.

Oppenheimer, C., Moretti, R., Kyle, P., Eschenbacher, A., Lowenstern, J., Hervig, R., Dunbar, N.W., 2011. Mantle to surface degassing of alkalic magmas at Erebus volcano, Antarctica. Earth Planet. Sci. Lett. 306, 261–271. http://dx.doi.org/10.1016/j.epsl.2011.04.005.

Optech, 2009. ILRIS Summary Specification Sheet. http://www.optech.ca/pdf/ILRIS_SpecSheet_110309_Web.pdf (accessed on: 11/15/2009).

Otway, P.M., Blick, G.H., Scott, B.J., 1994. Volcanic deformation modeling of Mount Erebus: methods and results of geodetic surveys, 1980–1985. In: Kyle, P.R. (Ed.), Volcanological and Environmental Studies of Mount Erebus, Antarctica. Antarctic Research Series 66, pp. 57–68. http://dx.doi.org/10.1029/ar066p0057.

Pavez, A., Remy, D., Bonvalat, S., Diament, M., Gabalda, G., Froger, J.-L., Julien, P., Legrand, D., Moisset, D., 2006. Insight into ground deformations at Lascar volcano (Chile) from

SAR interferometry, photogrammetry and GPS data: implications on volcano dynamics and future space monitoring. Remote Sens. Environ. 100, 307–320. http://dx.doi.org/10.1016/j.rse.2005.10.013.

Pesci, A., Fabris, M., Conforti, D., Loddo, F., Baldi, P., Anzidei, M., 2007. Integration of ground-based laser scanner and aerial digital photogrammetry for topographic modelling of Vesuvio volcano. J. Volcanol. Geotherm. Res. 162 (3), 123–138.

Pesci, A., Teza, G., Bonali, E., 2011. Terrestrial laser scanner resolution: numerical simulations and experiments on spatial sampling optimization. Remote Sens. 3, 167–184.

Pesci, A., Teza, G., Casula, G., Fabris, M., Bonforte, A., 2013. Remote sensing and geodetic measurements for volcanic slope monitoring: surface variations measured at northern flank of La Fossa Cone (Vulcano Island, Italy). Remote Sens. 5 (5), 2238–2256.

Peters, N., Oppenheimer, C., Killingsworth, D.R., Frechette, J., Kyle, P., 2014a. Correlation of cycles in lava lake motion and degassing at Erebus Volcano, Antarctica. Geochem. Geophys. Geosyst. 15. http://dx.doi.org/10.1002/2014GC005399.

Peters, N., Oppenheimer, C., Kyle, P., Kingsbury, N., 2014b. Decadal persistence of cycles in lava lake motion at Erebus volcano, Antarctica. Earth Planet. Sci. Lett. 395, 1–12.

Petrie, G., Toth, C.K., 2008. Introduction to laser ranging, profiling, and scanning. In: Shan, J., Toth, C.K. (Eds.), Topographic Laser Ranging and Scanning: Principles and Processing. CRC Press, Taylor & Francis http://dx.doi.org/10.1201/9781420051438.ch1 (590 pp.).

Stevenson, D.S., Blake, S., 1998. Modelling the dynamics and thermodynamics of volcanic degassing. Bull. Volcanol. 60, 307–317.

Sweeney, D., Kyle, P.R., Oppenheimer, C., 2008. Sulfur dioxide emissions and degassing behavior of Erebus volcano, Antarctica. J. Volcanol. Geotherm. Res. 177, 725–733. http://dx.doi.org/10.1016/j.jvolgeores.2008.01.024.

Tarolli, P., 2014. High-resolution topography for understanding Earth surface processes: opportunities and challenges. Geomorphology 216, 295–312.

Tarquini, S., Favalli, M., Mazzarini, F., Isola, I., Fornaciai, A., 2012. Morphometric analysis of lava flow units: case study over LIDAR-derived topography at Mount Etna, Italy. J. Volcanol. Geotherm. Res. 235, 11–22.

Witham, F., Woods, A.W., Gladstone, C., 2006. An analogue experiment model of depth fluctuations in lava lakes. Bull. Volcanol. 69, 51–56. http://dx.doi.org/10.1007/s00445-006-0055-8.

Zandomeneghi, D., Aster, R., Kyle, P., Barclay, A., Chaput, J., Knox, H., 2013. Internal structure of Erebus volcano, Antarctica imaged by high-resolution active-source seismic tomography and coda interferometry. J. Geophys. Res. 118, 1067–1078. http://dx.doi.org/10.1002/jgrb.50073.

Zhu, L., Mu, Y., Shi, R., 2008. Study on the resolution of laser scanner point cloud. Proceedings of 2008 IEEE International Geoscience & Remote Sensing Symposium, July 2008, Boston, MA, USA vol. 2. IEEE, Piscataway, NJ, USA, pp. 1136–1139. http://dx.doi.org/10.1109/igarss.2008.4779200.